



ARTICLE

WILEY

Synthesis and combustion catalytic activity of ferrocene-based energetic compounds

Shiqi Huang¹ | Rong Yang¹ | Jiaodan Wang¹ | Shuai Chang² |
Xiaofeng Gou¹  | Chengwen Hua¹ | Junlong Zhao¹ 

¹Key Laboratory of Synthetic and Natural Functional Molecule Chemistry of Ministry of Education, College of Chemistry and Materials Science, Northwest University, Shaanxi, China

²School of Physics, Northwest University, Shaanxi, China

Correspondence

Junlong Zhao, Key Laboratory of Synthetic and Natural Functional Molecule Chemistry of Ministry of Education, College of Chemistry and Materials Science, Northwest University, Shaanxi 710127, China.
Email: zhaojunlong327@163.com

Funding information

the National Natural Science Foundation of China, Grant/Award Number: 21703171; the Natural Science Basic Research Plan in Shaanxi Province of China, Grant/Award Number: 2018JQ2043; the Foundation of Shaanxi Educational Committee, Grant/Award Number: 19JS063

Abstract

Ammonium perchlorate (AP) is a common oxidizer in composite solid rocket propellants due to its excellent burning characteristics, good processability, and storability. Owing to their outstanding catalytic effects, ferrocene, and its derivatives have become the most widely used burning rate catalysts (BRCs). The addition of ferrocene and its derivatives to AP rendered performance optimization. In this study, azole-based ferrocenyl compounds were successfully synthesized. The compounds were characterized by single-crystal X-ray diffraction, UV-vis spectroscopy, and other techniques. The thermal degradation of AP catalyzed by these compounds was evaluated by differential scanning calorimetry and thermogravimetric analysis. Results revealed that the decomposition peak temperature of AP dramatically decreases and that the released heat of AP significantly increases with the new compounds as additives. Hence, the six azole-based ferrocenyl BR catalysts are favorable for the combustion catalytic activity.

1 | INTRODUCTION

Solid propellants are important in the military and aerospace fields.^[1] An excellent solid propellant must exhibit an extremely stable burning rate between certain boundaries at a given operating pressure, a low pressure index, and a low characteristic signal during burning.^[2] The addition of a burning rate catalyst (BRC) into a solid propellant is key to achieving these goals.^[3] Several BRCs have been reported, including metal complexes,^[4] carbon black, and related compounds,^[5] transition-metal oxides,^[6] nanomaterials,^[7] and ferrocene and its derivatives.^[8] Ferrocene (Fc) and its derivatives have been

widely used in several fields such as medicine,^[9] biology, agriculture, catalysis,^[10] and materials,^[11] especially, Fc-based BRCs have attracted considerable attention due to their excellent BRC activity, broad range of BR adjustments, and facile compatibility with an organic binder. Their efficient BR catalytic performance is derived from highly active Fe₂O₃, which decomposes during combustion.^[12] In recent years, several nitrogen-rich ferrocene compounds have been synthesized. These compounds not only exhibit an excellent combustion catalytic activity and favorable mechanical performance but also exhibit a low pressure index.^[13] In 2013, Bian and co-workers^[14] have prepared complexes with 1,2,3-(NH)-triazolylferrocene derivatives and copper(II) and zinc(II), and their catalytic performance for the thermal

Shiqi Huang and Rong Yang contributed equally to this study.

decomposition of ammonium perchlorate (AP) has been investigated by thermogravimetric analysis and differential thermal analysis. Results revealed that the complexes exhibit a distinct effect on the high-temperature decomposition (HTD) of AP, and the temperature shifts down to 32.3°C to 61.9°C. In 2015, Zhang^[15] has introduced novel ionic compounds synthesized using 1-(ferrocenylmethyl)-imidazolium cations and the polycyano anion, and the results revealed that the decomposition temperature span of the AP is narrowed; HTD peaks shift down to 74.2°C to 120.7°C; and the release heat is 1156.6 to 2164.0 J/g. In 2016, Zhang^[16] has used alkali hydroxides or carbonates to deprotonate 5-ferrocenyl-1H-tetrazole, affording the corresponding metal salts. Results revealed that the complexes exhibit a distinct effect on HTD and HTD peaks with a downward shift to 61.3°C to 85.2°C, and the release heat is in the range of 1339.9 to 1946.3 J/g. In 2019, Zhang and co-workers^[17] synthesized more than 20 ferrocene compounds, which were synthesized by copper-catalyzed azide alkyne cycloaddition reactions. Results revealed that the new ferrocene-based compounds have high thermal stability and the new ferrocenyl compounds exhibit high catalytic activity in the thermal degradation of AP during their combustion. Energetic combustion catalysts are very distinctive in many types of BRCs.^[18] Energetic compounds have been widely used in solid propellants due to their high nitrogen content, high tension, high heat of formation, facile oxygen balance, and environmental friendliness.^[19] Novel high-nitrogen energetic derivatives such as azoles, dioxazines, and polynitro compounds have provided a new research direction for energetic compounds in new types of BRCs. Generally, novel BRCs should exhibit a well-controlled BR of propellants, excellent mechanical performance, low signal characteristics, and environmental friendliness. As typical nitrogen-rich energy compounds, azoles comprise several N=N bonds and C—N bonds. They can maintain a high energy level, high density, and good thermal stability, in addition, they can increase the nitrogen content and provide energy for solid propellants. In this study, ferrocenyl-based energetic compounds and a ferrocenyl-based energetic oligomer are prepared using two novel BR catalysts, where the ferrocenyl groups are modified with azoles: Class A, comprising a nitrogen-containing heterocyclic ring directly linked to 1,1'-ferrocenyl methanone and class B, where the amino group on the nitrogen-containing heterocyclic ring is connected to 1,1'-ferrocenyl methanone. In addition, catalytic effects of the compounds on the thermal decomposition of AP were investigated to confirm their potential BRC activities.

2 | RESULTS AND DISCUSSION

2.1 | Single-Crystal Determination

To obtain structural information about the new compounds, their single crystals were grown, but only single crystals of two compounds **A1** and **B2** were successfully collected and characterized by single X-ray crystallography. **A1** exhibited a cis structure and crystallized in the monoclinic space group P_{21}/c (Figure 1). The pyrazole ring, carbonyl group, and ferrocene Cp rings were almost present in the same plane. The distances of C—N bonds (C15—N3, C6—N1) generated by 1,1'-ferrocenedicarbonyl chloride and pyrazole were 1.405(5) and 1.401(5) Å, respectively. The distance between two pyridines was 3.5749 Å, with strong π - π stacking interactions.

B1 crystallized in the hexagonal space group $P6_5$. The comparison of **B2** with **A1** revealed different structures. 1,2,4-Triazole and the Cp ring were almost present in the vertical plane. The distances of C—N bonds (C14—N5, C6—N1) generated by 1,1'-ferrocenedicarbonyl chloride and 4-amine-1,2,4-triazole were 1.351(7) and 1.365(7) Å, respectively. The C—N bond of **A1** was shorter than that of **B1**, so the bond of **A1** is more stable. **B2** and water molecules participated in intramolecular strong hydrogen bonding [N5—H6...O4, O3—H3A...O1, O4—H4B...N4, and N1—H1...N8] to form a two-dimensional supramolecular structure. The presence of a large number of hydrogen bonds in the molecules led to stable compounds (Figure 2).

2.2 | UV-vis absorption spectra

Figure 3 shows the UV-vis absorption spectra of all compounds in DMSO. Absorption bands were observed near 280 nm for **A1**–**A3**, corresponding to π - π^* transitions of

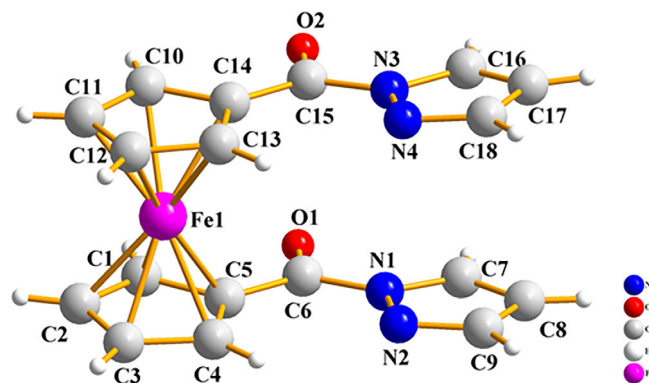


FIGURE 1 Single-crystal structure of compound **A1**

FIGURE 2 a, Single-crystal structure of compound **B2**, b, two-dimensional supramolecular structure of **B2** (The green dashed line represents the hydrogen bond.)

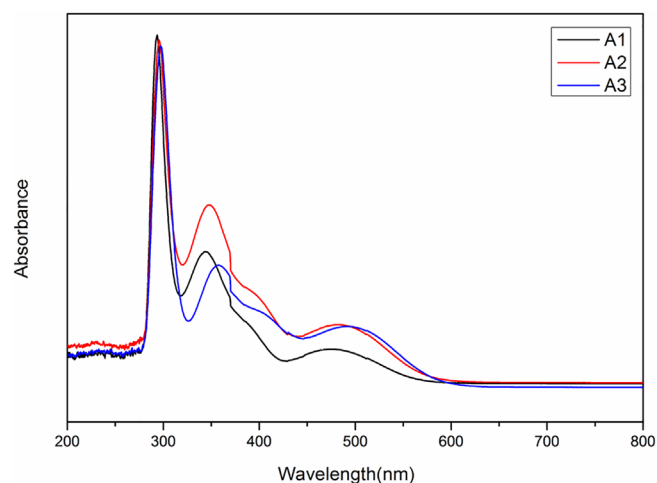
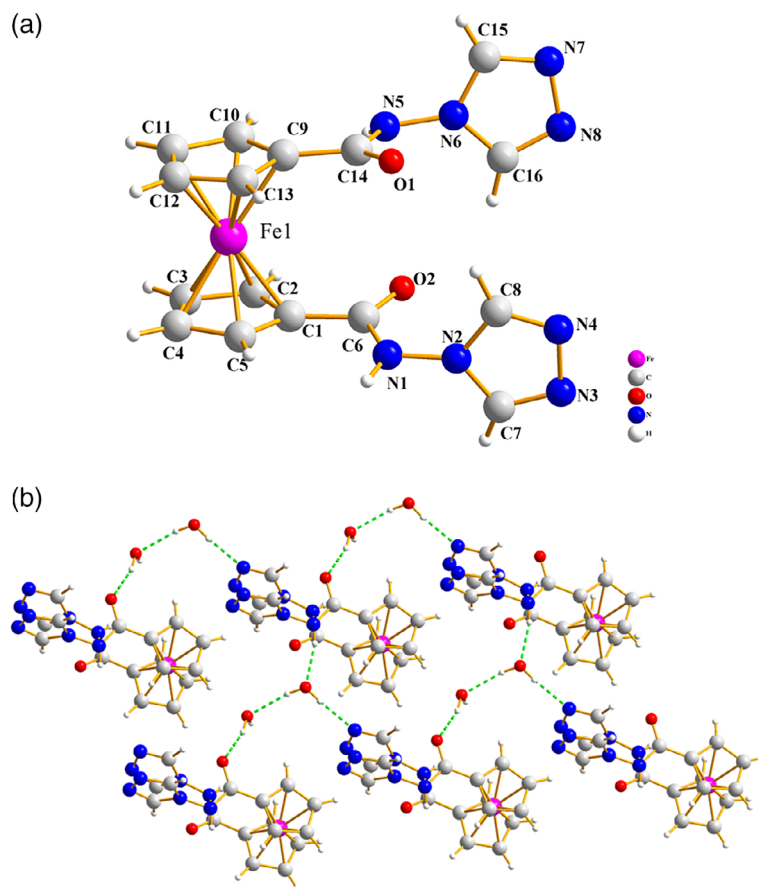


FIGURE 3 UV-vis spectra of compounds **A1-A3**

Cp rings and absorption bands near 350 nm corresponded to the MLCT transition. Strong, broad bands observed from 320 to 420 nm corresponded to $n-\pi^*$ transitions of the carbonyl group, which red-shifted due to the conjugation of the carbonyl group with nitrogen-containing heterocycles. Broad, weak bands ranging from

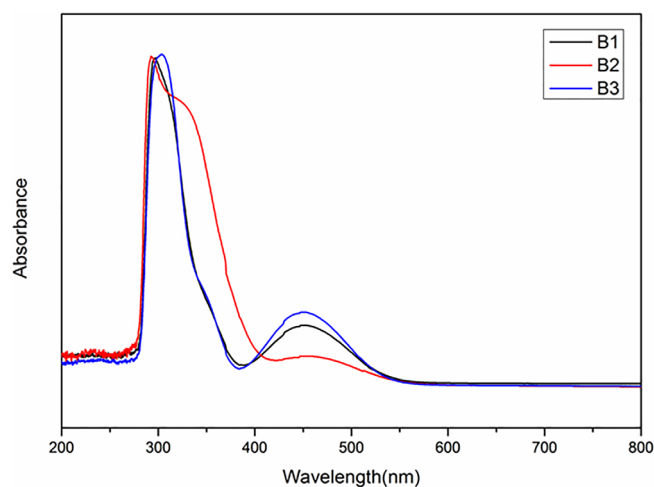


FIGURE 4 UV-vis spectra of compounds **B1-B3**

400 to 550 nm corresponded to d-d transitions of the Fe atom.

Absorption bands near 280 nm for **B1-B3** corresponded to $\pi-\pi^*$ transitions of Cp rings and absorption bands near 350 nm corresponded to the MLCT transition. Broad, weak bands in the range from 400 to 550 nm

corresponded to the d-d transitions of the Fe atom (Figure 4).

2.3 | Thermal stability studies of ferrocenyl-based energetic compounds

Thermal stability is an important property for energetic catalytic materials, where the effect of materials under a specific temperature program can be examined. Figures 5 and 6 show the TG curves of **A1-A3** and **B1-B3**, respectively. **A1** and **A2** exhibited three weight-loss processes, first starting from 118°C to 119°C and ended at 171°C; second at 186°C with a mass loss of 7.1%; and third at 11.1%, possibly related to the volatilization of water. The second weight loss was observed from 215°C, 230°C, and ended at 328°C, 457°C, with mass losses of ~18.5% and 19.6%, related to the dissociation of the amide bond. The third weight loss was observed at 380°C, from 671°C to 601°C, 761°C with mass losses of ~14.3% and ~13.0%, probably related to the collapse of ferrocene. The first stage for A3 was observed at 169°C to 197°C, displaying a rapid weight loss process of ~36.2% due to the dissociation of the amide bond; the second stage from 458°C to 662°C, with a weight-loss process of ~16.7% caused by the collapse of ferrocene. The final residues for each compound should be Fe_2O_3 and carbon. The thermal decomposition of class A was a rapid process, where the amide bond was first dissociated during the temperature increase. With the further increase in the temperature, ferrocene collapsed. In the five-membered aromatic heterocyclic system, all nitrogen atoms belonged to pyridines, with the aromatic ring being the electron-deficient system. With the increase in the amount of nitrogen atoms, the conjugated effect became increasingly weaker, and the stability of the compound deteriorated.

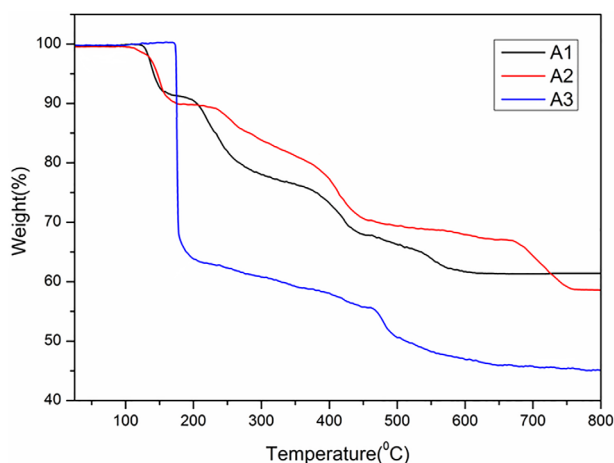


FIGURE 5 TG curves of compounds **A1-A3**

B1 exhibited a slow weight-loss process, where it was stabilized before 143°C. With the increase in the temperature, a mass loss of 44.7% at 497°C was observed due to the dissociation of the amide bond. **B2** was divided into two stages. The first stage was observed at 158°C to 257°C, with a mass loss of 31.4%, corresponding to the dissociation of the amide bond. The second mass loss of ~25% was observed at 256°C to 441°C, corresponding to the collapse of ferrocene. **B3** exhibited a slow weight-loss process at 208°C to 475°C, with a mass loss of ~62% caused by the collapse of ferrocene.

2.4 | Catalytic effect on the decomposition of ammonium perchlorate

AP is the most widely used high-energy oxidant in solid propellants. The combustion of a composite solid propellant is strongly dependent on the thermal decomposition of AP. Generally, the catalytic performance of BRCs in a solid propellant is typically evaluated by their effects on the thermal decomposition of AP according to DSC. The DSC curve for the thermal decomposition of pure AP revealed one endothermic peak and two exothermic peaks (Figure 7). The endothermic peak at 242°C corresponded to the morphological transition from an orthorhombic to a cubic phase of AP. The first exothermic peak at 337 corresponded to low-temperature decomposition (LTD). The second exothermic peak at 442°C corresponded to HTD. The mass ratio of the ferrocene energetic compound to AP was 1:3. The morphological-transition endothermic peak of **A1-A3** disappeared, and two exothermic peaks were observed; both LTD and HTD stages of AP were significantly changed by the inclusion of additives (Figure 8). The additive led to the narrowing of the decomposition temperature span of AP; two exothermic

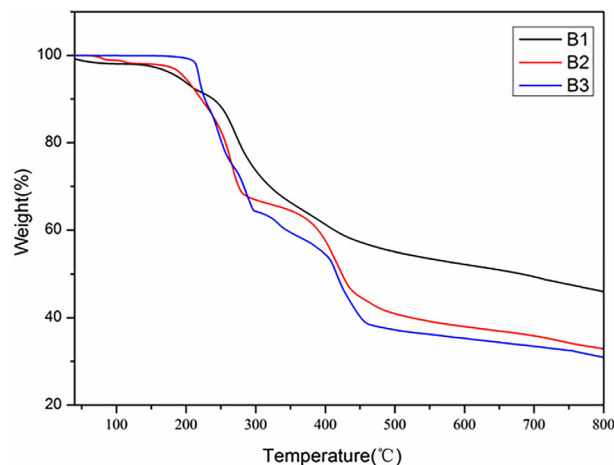


FIGURE 6 TG curves of compounds **B1-B3**

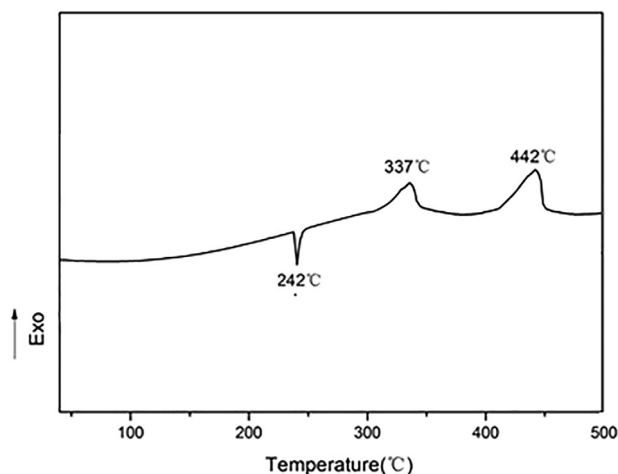


FIGURE 7 DSC curve of pure AP

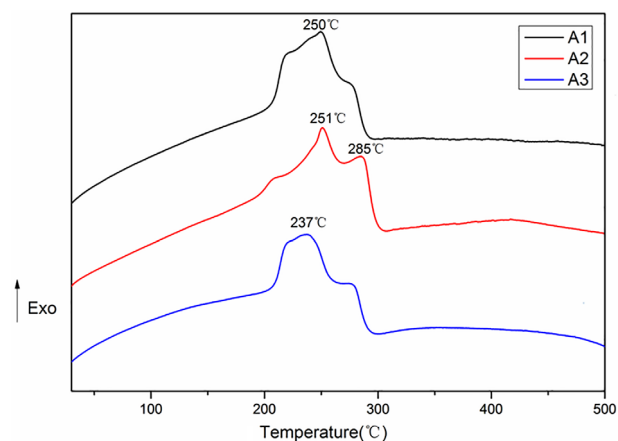


FIGURE 8 DSC curves of A1-A3

peaks in **A1** were combined into one broad exothermic peak; and two exothermic peaks of **A2** did not completely merge, but the exothermic peak was the sharpest. The exothermic peak of **A3** was the most decentralized. Thus, these new compounds exhibit a distinct positive catalytic effect on the LDT and HDT stages of AP. From the released heat of AP added into **A1** (2875 J/g), **A2** (2931 J/g), and **A3** (2976 J/g), the catalytic activity of **A1** was weaker than that of **A2**, and that of **A2** was weaker than that of **A3**. With the increase in the nitrogen content, the three compounds released more heat. **B1**, **B2**, and **B3** exhibited no effect on the morphological transition peak, and the temperature was constant at 244°C to 247°C (Figure 9). The two exothermic peaks in **B1** and **B2** at 300°C and 289°C, respectively, combined into one sharp exothermic peak. Compared to pure AP, **B1** LDT peaks shifted up to ~37°C, HDT peaks shifted down by ~142°C; **B2** LDT peaks shifted down by ~48°C, and HDT peaks

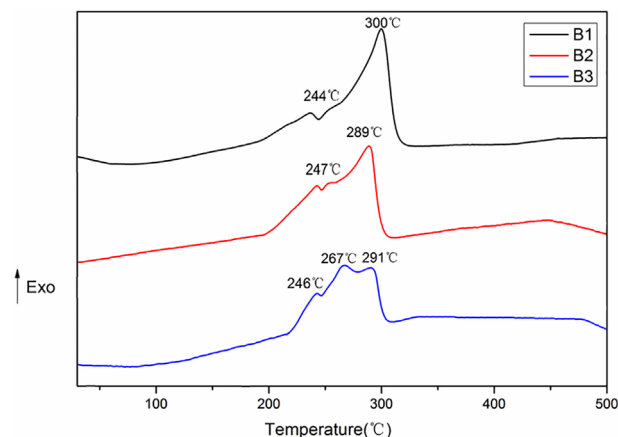


FIGURE 9 DSC curves of B1-B3

decreased to ~153°C. The released heat values for AP added **B1** and **B2** were 2493 J/g and 2895 J/g, respectively. **B3** exhibited two closed peaks with LDT and HDT peaks, which shifted down to ~70°C and 151°C, respectively, with a released heat of 2589 J/g. With the increase in the nitrogen content, the energy released by these three compounds also increases. At the same nitrogen content, irrespective of the presence of absence of the methyl group, heat release was affected, containing methyl can decrease heat.

3 | CONCLUSIONS

In summary, six azole-based ferrocenyl compounds were successfully synthesized and characterized. Single-crystal X-ray diffraction analysis and other characterization techniques confirmed the molecular structures of the prepared products. These azole-based ferrocenyl compounds exhibited high catalytic activity for the thermal degradation of ammonium perchlorate. Both A and B compounds advance the thermal decomposition peak temperature of AP, but A compounds advance more. In terms of releasing heat, Class B compounds release more concentrated heat than class A compounds, because Class A compound is more rigid than Class B compound, so the molecular structure is more likely to collapse after heating, interacting with AP, and forming Fe atoms when exposed the highly active ferric oxide catalyzes the further decomposition of AP.

Experimental Section Caution: Azole compounds are hazardous materials, and explosion may occur under certain conditions. Necessary safety precautions (such as safety glasses, a face shield, and a plastic spatula) should be used during the experiment, especially during the large-scale preparation of such compounds.

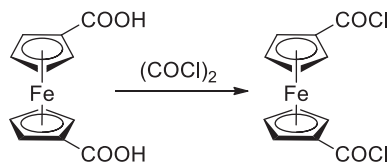
3.1 | Materials and instruments

All commercially available reagents were used without any purification. The IR spectrum of compounds was recorded by the KBr pellet method on a Bruker FTIR spectrometer. NMR spectra were recorded on a Bruker AVANCE III-400 MHz spectrometer and a Bruker Ascend 400 MHz spectrometer. TG and DSC analyses were performed on a Netzsch STA 449C instrument using nitrogen gas as the atmosphere. First, 1 to 3 mg of samples was added into the crucible for measurements. Specific procedures were described as follows: Standard weights were used for the calibration of the balance. At 25°C to 800°C, the baseline was calibrated by using an empty crucible at a heating rate of 20°C·min⁻¹ and a nitrogen gas flow rate of 10 mL·min⁻¹.

3.2 | Synthesis

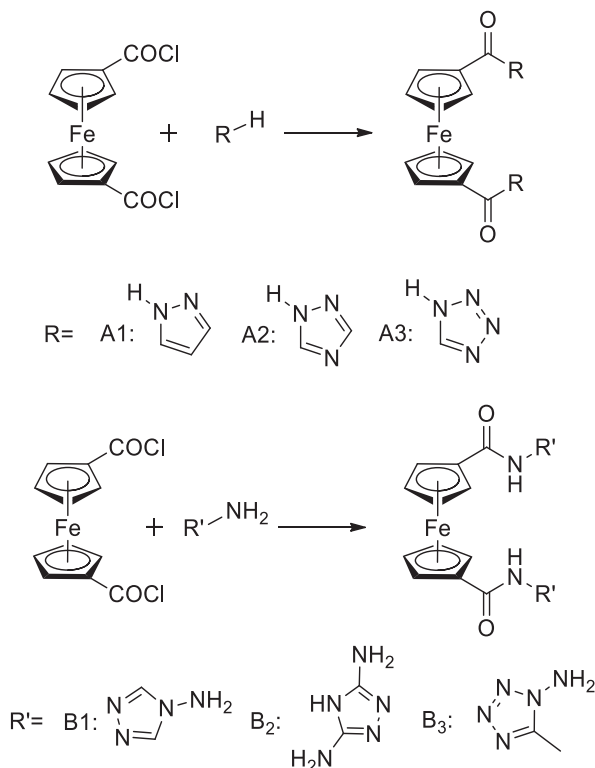
For the preparation of ferrocene dicarbonyl chloride, acyl chloride was easily hydrolyzed; hence, the solvent needs to be dried, and the reaction is carried out under dry conditions to increase the yield. Acetonitrile and triethylamine were selected as the solvent and acid-binding agent, respectively, and the temperature was maintained at 40°C during the reaction.

3.3 | Synthesis of ferrocene dicarbonyl chloride (FDC)

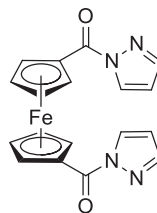


FDC was synthesized by an optimized procedure.^[20] First, 1,1'-ferrocenedicarboxylic acid (2.74 g, 0.01 mmol) was dissolved in a dry dichloromethane (50 mL) and dimethylformamide (0.15 mL) solution. After adding 20 mL of dry dichloromethane into a constant-pressure dropping funnel, 3 mL of oxalyl chloride was rapidly added. This mixed solvent was controlled to drip within 0.5 hour. Next, the mixture solution was stirred at 25°C for 0.5 hour, followed by heating at reflux for 10 hours. All procedures were monitored by TLC. The precipitate was collected and dried by reduced pressure distillation. To obtain a high-purity product, the precipitate was recrystallized using a mixture of 50 mL of petroleum ether-dichloromethane (petroleum ether:dichloromethane = 1:1), affording a red solid in 95% yield.

3.4 | Synthesis of new compounds



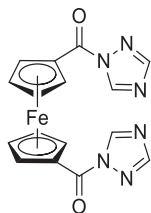
FDC was prepared by using an optimized procedure.^[21] Synthetic procedures for compounds **A1-A3** as well as **B1-B3** were similar; hence, the preparation for **A1** is shown as an example. First, 15 mL of acetonitrile with 1,1'-ferrocenedicarbonyl chloride (15.547 g, 0.05 mol) was added with stirring into a 50 mL round-bottom flask with containing acetonitrile (15 mL) and 1H-pyrazole (6.808 g, 0.1 mol). Second, the mixed solution was stirred at 40°C for 10 hours. All procedures are monitored by TLC. The precipitate was collected by filtration and dried at 40°C under vacuum.



3.4.1 | 1,1'-Ferrocenylbis ((1H-pyrazol-1-yl) methanone) (A1)

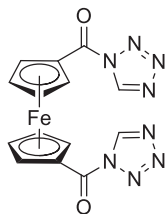
The product was obtained through recrystallization from acetonitrile, as a red blocks, yield: 80%, m.p. 119°C to 121°C; ¹H NMR (400 MHz, DMSO-*d*₆) δppm: 8.39 (s, 2H, CH), 7.81 (s, 2H, CH), 6.56 (s, 2H, CH), 5.38 (s, 4H, C₅H₄), 4.77 (s, 4H, C₅H₄); ¹³C NMR (100 MHz, DMSO-

d_6) δ ppm: 168.2 (CO), 144.7 (NCH), 129.8 (NHCH), 109.5 (NHCHCH), 75.2, 74.5, 73.1 (C₅H₄). IR (KBr): 3120, 2880, 2642, 2556, 1687, 1505, 1410, 1295, 1171, 1027, 913, 827, 731 cm⁻¹. HRMS (ESI) m/z calculated for C₁₈H₁₄FeN₄O₂ [M + Na⁺]: 397.0364; found: 397.0354.



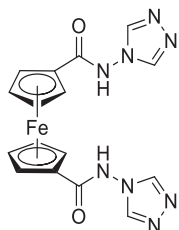
3.4.2 | 1,1'-Ferrocenylbis ((1H-1,2,4-triazol-1-yl) methanone) (A2)

The product was obtained through recrystallization from acetonitrile, as a red blocks, yield: 83%, m.p. 160°C to 162°C; ¹H NMR (400 MHz, DMSO-*d*₆) δ ppm: 9.33 (s, 2H, CH), 8.25 (s, 2H, CH), 5.39 (s, 4H, C₅H₄), 4.89 (s, 4H, C₅H₄); ¹³C NMR (100 MHz, DMSO-*d*₆) δ ppm: 166.8 (CO), 153.6 (CONNCH), 145.8 (CONCH), 75.7, 75.3, 72.2 (C₅H₄). IR (KBr): 3110, 2880, 2642, 2556, 1678, 1487, 1440, 1305, 1162, 1037, 904, 827, 741 cm⁻¹. HRMS (ESI) m/z calculated for C₁₆H₁₂FeN₆O₂ [M + Na⁺]: 399.0269; found: 399.0278.



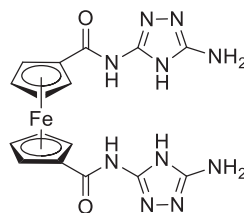
3.4.3 | 1,1'-Ferrocenylbis ((1H-tetrazol-1-yl) methanone) (A3)

The product was obtained through recrystallization from acetonitrile, as a red blocks, yield: 70%, m.p. 169°C to 171°C; ¹H NMR (400 MHz, DMSO-*d*₆) δ ppm: 10.13 (s, 2H), 5.45 (s, 4H, C₅H₄), 5.07 (s, 4H, C₅H₄); ¹³C NMR (100 MHz, DMSO-*d*₆) δ ppm: 165.4 (CO), 144.1 (NCH), 76.8, 75.2, 71.8 (C₅H₄). IR(KBr): 3120, 2871, 2642, 2556, 1677, 1486, 1295, 1151, 1018, 913, 827, 741 cm⁻¹. HRMS (ESI) m/z calculated for C₁₄H₁₀FeN₈O₂ [M + Na⁺]: 401.0174; found: 401.0179.



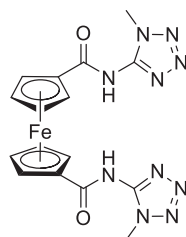
3.4.4 | N,N'-bis(4H-1,2,4-triazol-4-yl)ferrocenecarboxamide (B1)

The product was obtained through recrystallization from the mixture (V_{EtOH}: V_{H₂O} = 1:1), as a red needles, yield: 95%, m.p. 240°C to 242°C; ¹H NMR (400 MHz, DMSO-*d*₆) δ ppm: 11.61(s, 2H, NH), 8.72(s, 4H, CH), 5.06 (s, 4H, C₅H₄), 4.70 (s, 4H, C₅H₄); ¹³C NMR (100 MHz, DMSO-*d*₆) δ ppm: 168.8 (CO), 144.3 (NCH), 73.9, 73.2, 71.0 (C₅H₄). IR (KBr): 3425, 3196, 3120, 1659, 1496, 1391, 1286, 1208, 1123, 1046, 1066, 923, 875, 817 cm⁻¹. HRMS (ESI) m/z calculated for C₁₆H₁₄FeN₈O₂ [M + H⁺]: 407.0667; found: 407.0678.



3.4.5 | N,N'-bis(3-amino-1H-1,2,4-triazol-5-yl)ferrocenecarboxamide (B2)

The product is obtained from the reaction without further purification, as a red solid, yield: 93%, m.p. 136°C to 138°C; ¹H NMR (400 MHz, DMSO-*d*₆) δ ppm: 4.70 (s, 4H, C₅H₄), 4.46 (s, 4H, C₅H₄); ¹³C NMR (100 MHz, DMSO-*d*₆) δ ppm: 171.2 (CO), 73.9, 72.9, 72.3 (C₅H₄). IR(KBr): 3408, 3129, 2633, 2548, 1689, 1495, 1409, 1301, 1172, 1044, 914, 840, 753 cm⁻¹. HRMS (ESI) m/z calculated for C₁₆H₁₆FeN₁₀O₂ [M + H⁺]: 437.0885; found: 437.0887.



3.4.6 | N,N'-bis(1-methyl-1H-tetrazol-5-yl)ferrocenecarboxamide (B3)

The product was obtained through recrystallization from the mixture (V_{EtOH}: V_{H₂O} = 1:1), as a yellow needles, yield: 94%, m.p. 142°C to 144°C; ¹H NMR (400 MHz, DMSO-*d*₆) δ ppm: 4.71 (s, 4H, C₅H₄), 4.47 (s, 4H, C₅H₄), 3.76 (s, 6H, CH₃); ¹³C NMR (100 MHz, DMSO-*d*₆) δ ppm: 171.7 (CO), 155.3 (NHC), 73.9, 73.0, 71.8 (C₅H₄), 32.3 (CH₃). IR (KBr): 3320, 3138, 2984, 1668, 1591, 1477, 1285,

1171, 1085, 894, 741 cm^{-1} . HRMS (ESI) m/z calculated for $\text{C}_{16}\text{H}_{16}\text{FeN}_{10}\text{O}_2$ [$\text{M} + \text{H}^+$]: 437.0885; found: 437.0887.

ACKNOWLEDGMENTS

The financial support by the National Natural Science Foundation of China (project 21703171), the Natural Science Basic Research Plan in Shaanxi Province of China (project 2018JQ2043), and the Foundation of Shaanxi Educational Committee (project 19JS063) is gratefully acknowledged.

ORCID

Xiaofeng Gou  <https://orcid.org/0000-0002-2946-9457>

Junlong Zhao  <https://orcid.org/0000-0002-6204-8929>

REFERENCES

- [1] (a) Y. Zhao, X. H. Zhang, W. Zhang, H. Xu, W. Xie, J. Du, Y. Liu, *J. Phys. Chem. A* **2016**, *120*, 765. (b) J. M. Gao, L. Wang, H. J. Yu, A. G. Xiao, W. B. Ding, *Propell. Explos. Pyrot.* **2011**, *36*, 404. (c) X. S. Gu, S. B. Xie, Q. Chen, S. Chen, H. Zhao, Z. Bian, *New J. Chem.* **2018**, *42*, 13319-13328.
- [2] X. L. Liu, J. Z. Li, F. Q. Bi, W. Zhang, G. Zhang, Z. Gao, *Eur. J. Inorg. Chem.* **2015**, *2015*, 1496.
- [3] (a) J. M. Gao, L. Wang, H. J. Yu, A. G. Xiao, W. B. Ding, *Propell. Explos. Pyrot.* **2011**, *36*, 404. (b) N. Zhang, J. Z. Li, G. F. Zhang, Z. Gao, *Z. Anorg. Allg. Chem.* **2018**, *644*, 337.
- [4] J. S. Wang, Y. Liu, H. B. Zhao, J. Liu, D. Y. Wang, Y. P. Song, Y. Z. Wang, *Polym. Degrad. Stab.* **2009**, *94*, 625.
- [5] J. P. A. Neef, M. Makkee, J. A. Moulijn, *Fuel* **1998**, *77*, 111.
- [6] I. P. S. Kapoor, P. Srivastava, G. Singh, *Propell. Explos. Pyrot.* **2009**, *34*, 351.
- [7] (a) P. R. Patil, V. N. Krishnamurthy, S. S. Joshi, *Propell. Explos. Pyrot.* **2006**, *31*, 442. (b) P. R. Patil, V. N. Krishnamurthy, S. S. Joshi, *Propell. Explos. Pyrot.* **2008**, *33*, 266. (c) A. A. Vargeese, K. Muralidharan, V. N. Krishnamurthy, *Propell. Explos. Pyrot.* **2015**, *40*, 260.
- [8] (a) N. Dilsiz, A. Ünver, *J. Appl. Polym. Sci.* **2006**, *101*, 2538. (b) A. Ünver, N. Dilsiz, M. Volkan, G. Akoz, *J. Appl. Polym. Sci.* **2005**, *96*, 1654. (c) J. B. Zhuo, H. D. Li, C. X. Lin, L. L. Xie, S. Bai, Y. F. Yuan, *J. Mol. Struct.* **2014**, *1067*, 112.
- [9] S. S. Braga, A. M. S. Silva, *Organometallics* **2013**, *32*, 5626.
- [10] (a) D. J. Young, S. W. Chien, T. S. A. Hor, *Dalton Trans.* **2012**, *41*, 12655-12665. (b) D. Schaarschmidt, H. Lang, *Organometallics* **2013**, *32*, 5668.
- [11] (a) A. W. Orbaek, N. Aggarwal, A. R. Barron, *J. Mater. Chem. A* **2013**, *1*, 14122-14132. (b) G. Huang, J. Weng, *Curr. Org. Chem.* **2011**, *15*, 3653. (c) V. Skrypnik, D. Rochefort, *Electrochim. Acta* **2019**, *305*, 155.
- [12] (a) W. Zhou, L. Wang, H. Yu, R. Tong, Q. Chen, J. Wang, X. Yang, Zain-ul-Abdin, M. Saleem, *Appl. Organomet. Chem.* **2016**, *30*, 796. (b) Y. Yuan, W. Jiang, Y. Wang, P. Shen, F. Li, P. Li, F. Zhao, H. Gao, *Appl. Surf. Sci.* **2014**, *303*, 354. (c) Z. Abdin, H. Yu, L. Wang, M. Saleem, H. Khalid, N. M. Abbasi, M. Akram, *Appl. Organomet. Chem.* **2014**, *28*, 567. (d) F. Xiao, F. Feng, L. Li, D. Zhang, *Propell. Explos. Pyrot.* **2013**, *38*, 358. (e) Zain-ul-Abdin, L. Wang, H. J. Yu, M. Saleem, M. Akram, H. Khalid, N. M. Abbasi, X. Yang, *J. Colloid Interface Sci.* **2017**, *487*, 38.
- [13] Z. Abdin, L. Wang, H. Yu, R. Tong, Q. Chen, J. Wang, X. Yang, M. S. Zain-ul-Abdin, *RSC Adv.* **2016**, *6*, 97469-97481.
- [14] H. Y. Zhao, L. Guo, S. F. Chen, Z. Bian, *RSC Adv.* **2013**, *3*, 19929-19932.
- [15] X. L. Liu, J. Z. Li, F. Q. Bi, W. Zhang, G. Zhang, Z. Gao, *Eur. J. Inorg. Chem.* **2015**, *2015*, 1496.
- [16] J. Z. Li, C. Y. Wang, X. N. Gao, F. Zhao, K. Zhao, X. Fan, G. Zhang, W. Zhang, Z. Gao, *Polyhedron* **2016**, *106*, 58.
- [17] W. Q. Cheng, X. L. Shi, Y. Zhang, Y. Jian, G. Zhang, *Inorg. Chim. Acta* **2020**, *502*, 119374.
- [18] (a) R. Wang, Y. Guo, Z. Zeng, J. M. Shreeve, *Chem. Commun.* **2009**, *19*, 2697. (b) Y. Yang, Y. Bai, F. Zhao, E. Yao, J. Yi, C. Xuan, S. Chen, *RSC Adv.* **2016**, *6*, 67308-67314. (c) D. Fischer, T. M. Klapötke, J. Stierstorfer, *Angew. Chem. Int. Ed.* **2015**, *54*, 10299-10302. (d) V. Thottampudi, F. Forohor, D. A. Parrish, J. M. Shreeve, *Angew. Chem. Int. Ed.* **2012**, *51*, 9881. (e) T. W. Myers, J. A. Bjorgaard, K. E. Brown, D. E. Chavez, S. K. Hanson, R. J. Scharff, S. Tretiak, J. M. Veauthier, *J. Am. Chem. Soc.* **2016**, *138*, 4685.
- [19] (a) Y. X. Tang, H. X. Gao, L. A. Mitchell, D. A. Parrish, J. M. Shreeve, *Angew. Chem. Int. Ed.* **2016**, *55*, 3200. (b) D. Fischer, T. M. Klapötke, J. Stierstorfer, *Angew. Chem. Int. Ed.* **2015**, *54*, 10299-10302. (c) T. J. Kealy, R. L. Pauson, *Nature* **1951**, *168*, 1039.
- [20] (a) S. Muhammad, H. J. Yu, L. Wang, K. Hamad, A. Muhammad, M. A. Nasir, Y. S. Chen, *J. Electroanal. Chem.* **2016**, *763*, 71. (b) V. Botla, C. Malapaka, *Org. Lett.* **2017**, *19*, 3528.
- [21] (a) D. Q. Liang, Y. N. Li, S. L. Gao, R. Li, X. Li, B. Wang, H. Yang, *Green Chem.* **2017**, *19*, 3344. (b) Z. G. Lv, B. N. Wang, Z. Y. Hu, *J. Org. Chem.* **2016**, *81*, 9924. (c) M. D. Reddy, A. N. Blanton, E. B. Watkins, *J. Org. Chem.* **2017**, *82*, 5080. (d) H. Hikawa, M. Imani, H. Suzuki, Y. Yokoyama, I. Azumaya, *RSC Adv.* **2014**, *4*, 3768. (e) G. T. Zhang, C. Liu, H. Yi, Q. Meng, C. Bian, H. Chen, J.-X. Jian, L.-Z. Wu, A. Lei, *J. Am. Chem. Soc.* **2015**, *137*, 9273. (f) H. M. Carlos, N. M. Jonathan, U. E. Godwin, P. K. Harry, A. Ibon, D. Christophe, *Eur. J. Med. Chem.* **2015**, *101*, 806.

SUPPORTING INFORMATION

Additional supporting information may be found online in the Supporting Information section at the end of this article.

How to cite this article: Huang S, Yang R, Wang J, et al. Synthesis and combustion catalytic activity of ferrocene-based energetic compounds. *J Heterocyclic Chem.* 2020;1-8. <https://doi.org/10.1002/jhet.3994>